

Impact of Chlorine on the Internal Transition Rates and Excited States of the Thermally Delayed Activated Fluorescence Molecule 3CzClIPN

Martin Streiter,¹ Tillmann G. Fischer,² Christian Wiebeler,^{3,4} Sebastian Reichert,¹ Jörn Langenickel,⁵ Kirsten Zeitler,² and Carsten Deibel*¹

¹*Institut für Physik, Technische Universität Chemnitz, 09126 Chemnitz, Germany*

²*Institut für Organische Chemie, Universität Leipzig, 04103 Leipzig, Germany*

³*Institut für Analytische Chemie, Universität Leipzig, 04103 Leipzig, Germany*

⁴*Leibniz-Institut für Oberflächenmodifizierung (IOM), 04318 Leipzig, Germany*

⁵*Zentrum für Mikrotechnologien, Technische Universität Chemnitz, 09126 Chemnitz, Germany*

NOTE: This document is the Accepted Manuscript version of a Published Work that appeared in final form in the Journal of Physical Chemistry C, copyright American Chemical Society after peer review and technical editing by the publisher. To access the final edited and published work see DOI: <https://doi.org/10.1021/acs.jpcc.0c03341>

ABSTRACT: We analyze internal transition rates and the singlet-triplet energy gap of the thermally activated delayed fluorescence (TADF) molecule 3CzClIPN, which recently was introduced as an efficient photocatalyst. Distribution and origin of the non-monoexponential decays, which are commonly observed in TADF films, are revealed by analysis of transient fluorescence with an inverse Laplace transform. A numerically robust global rate fit routine, which extracts all relevant TADF parameters by modeling the complete set of data, is introduced. To compare and verify the results, all methods are also applied to the well-known 4CzIPN. The influence of the molecular matrix is discussed by embedding low concentrations of TADF molecules in polystyrene films. Finally, quantum chemical calculations are compared to the experimental results to demonstrate that the chlorine atom increases the charge transfer character of the relevant states, resulting in a reduction of the singlet-triplet energy gap.

Keywords: TADF, 4CzIPN, 3CzClIPN, reverse intersystem crossing, transition orbitals

I. INTRODUCTION

State-of-the-art materials utilized in organic light-emitting diodes (OLED) and photocatalysis (PC) usually contain metal-complexes with rare elements such as iridium and ruthenium.^{1–4} Production cost, element scarcity and questions of environmentally friendly mining led to efforts in synthesizing metal-free molecules with comparable and therefore competitive photophysical and chemical properties. In OLED technology, internal quantum efficiencies of 100 % can be realized with traditional metal-complexes by triplet recombination (phosphorescence), overcoming the limitation of maximal 25 % internal quantum efficiency set by singlet spin statistics.⁵ By converting triplet states into singlet states, so-called TADF (thermally activated delayed fluorescence) materials can—without the necessity of a metal center—equally achieve up to 100 % internal quantum efficiency.⁶ In addition to prompt fluorescence emission from the singlet S_1 state back into the S_0 ground state (referred to as PF in the following), the T_1 triplet state (populated by intersystem crossing with rate k_{ISC}) can repopulate the S_1 state by reverse intersystem crossing (k_{RISC}), leading to delayed fluorescence (DF). TADF materials are characterized by a donor–acceptor structure which also can be realized by metal-free molecules. Localized wavefunctions on donor and acceptor sites are spatially and energetically well separated, usually by large dihedral angles between donor and acceptor groups. This design leads to a decrease of the energy difference ΔE_{ST} between excited

S_1 and T_1 state. These three parameters are theoretically connected by detailed balance in equation (1).⁷ The equation suggests that small ΔE_{ST} are favored in OLED design because of efficient singlet-from-triplet conversion as well as important in PC as an indicator of a strong charge transfer state character of the excited state. However, when ΔE_{ST} is too low, the exchange integral between ground and excited state approaches zero, leading to low absorption.⁸ Therefore, in both, OLED and PC applications, also parameters such as absorption, nonradiative losses, quantum yield and k_{RISC} need to be considered.

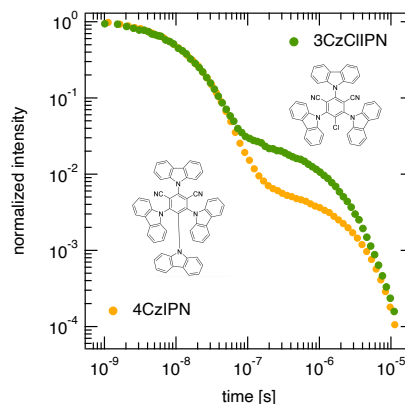


FIG. 1. Prompt and delayed fluorescence decay of 4CzIPN and 3CzClIPN films at room temperature.

$$k_{\text{RISC}} = k_{\text{ISC}} \exp\left(-\frac{\Delta E_{\text{ST}}}{k_{\text{B}}T}\right). \quad (1)$$

One of the most studied TADF molecule is 4CzIPN (1,2,3,5-tetrakis(carbazol-9-yl)-4,6-dicyanobenzene), which was introduced by Adachi *et al.*⁶ The four carbazole groups act as an electron donor attached to the electron accepting 4,6-dicyanobenzene core at an angle of 60°. Adachi *et al.* first demonstrated its efficient properties as a green OLED emitter.⁶ As a photocatalyst, 4CzIPN shows strong oxidative and reductive ground state potentials. Recently it was shown that modification of 4CzIPN to 3CzCIIPN increases the oxidative ground state potential demonstrating 3CzCIIPN as a potential alternative to the well-established, oxidizing photocatalyst Ir(dF-CF₃-ppy)₂(dtbbpy)(PF₆).^{9,10} While the influence of chlorine on TADF molecules is only partly discussed in the literature^{11,12}, little is known about the photophysical properties of the photocatalytically potent molecule 3CzCIIPN. In this paper, we elucidate how chlorine influences the internal transition rates and excited state energies by examining temperature-dependent fluorescence transients with two improved algorithms. Quantum chemical calculations and wavefunction analysis support the experimental results and explain the difference between the two molecules in detail.

II. METHODS

Photons emitted via PF and DF are energetically indistinguishable, as they both originate from S_1 (see SI). However, in time-dependent measurements, PF and DF can be separately analyzed as they occur on different timescales with different intensities. Precise and robust routines for measuring, evaluating and simulating TADF parameters are in the focus of current research.^{8,13–17} Figure 1 shows the time-dependent fluorescence and chemical structure of the two molecules in focus of this study, 4CzIPN and 3CzCIIPN.

We compare two improved evaluation methods based on the work of Dias¹⁴, Berberan-Santos^{18,19}, Penfold²⁰, Scholz²¹, Haase²² and respective co-authors. Both methods require only fluorescence transients without additional measurements of quantum yields, triplet quenching or phosphorescence. They are therefore experimentally straightforward and sensitive, allowing analysis of highly diluted films with weak emission towards projected single molecule measurements.

Dias *et al.* showed, that k_{RISC} can be estimated from fluorescence transient measurements when the yields of intersystem crossing and reverse intersystem crossing of the material are high.¹⁴ More specifically, for a DF/PF ratio larger than ≈ 4 (which can be determined from the integrals of both regimes in the transient fluorescence signal) and an assumed reverse intersystem crossing yield

approaching 100%, k_{RISC} can be estimated from transient measurements with a DF lifetime τ_{DF} by:

$$k_{\text{RISC}} = \frac{1}{\tau_{\text{DF}}} \left(1 + \frac{\int_0^\infty DF dt}{\int_0^\infty PF dt}\right). \quad (2)$$

To determine τ_{DF} and the integral DF/PF ratio (≈ 5 for 4CzIPN and ≈ 6 for 3CzCIIPN, therefore equation (2) was applicable), we analyzed our data with the RegSLapS algorithm which utilizes an inverse Laplace transform.²³ The spectral function g including the effective rates k_i for each component in the multiexponential decay L can be obtained by calculating the inverse Laplace transform of:

$$L(t, T) = \int_0^\infty g(k(T)) \exp(-k(T)t) dk. \quad (3)$$

The solution g contains information about the amplitudes A_i , effective rates k_i as well as the necessary number of components i . Subsequently, every decay can be fitted with the sum of multiple exponential functions (see SI),

$$L(t, T) = \sum_i A_i \exp(-k_i t). \quad (4)$$

This analysis is illustrated in figure 2 for the transient fluorescence of a neat 4CzIPN film and also applied to 3CzCIIPN at room temperature. Since solving of equation (3) is an ill-posed problem, the experimental data has to be almost noise free to avoid instability of the solution g . Additionally, uniqueness could not be given as different spectral functions g can have nearly the same Laplace transform. Therefore, we used an extended version of the Tikhonov's regularization as described by Reichert *et al.*²³ to search for the most stable and reasonable solutions.

With the integral of $A \exp(-kt)$ being Ak^{-1} and an effective DF rate²⁴ (see SI), k_{RISC} was calculated from the inverse Laplace transform with

$$k_{\text{RISC}} = \langle k_{\text{DF}} \rangle \left(1 + \frac{\sum A_i k_{i\text{DF}}^{-1}}{\sum A_j k_{j\text{PF}}^{-1}}\right). \quad (5)$$

Temperature-dependent values of k_{RISC} were evaluated according to equation (5), and the $k_{\text{RISC}}(T)$ plots (see SI) were then fitted with

$$k_{\text{RISC}} = k_{\text{A}} \exp\left(-\frac{\Delta E_{\text{ST}}}{k_{\text{B}}T}\right). \quad (6)$$

Note, that the prefactor k_{A} is described differently in the literature, as discussed later.^{6,7,16,25} We refer to this evaluation method as *Laplace fit* throughout the paper.

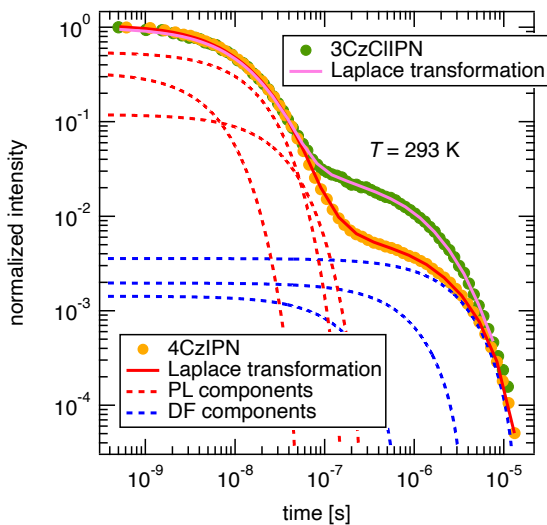


FIG. 2. Exemplary single components of the inverse Laplace transform algorithm. Resulting fits for neat 4CzIPN and 3CzCIIPN films at room temperature.

Next, we discuss our second method, the *global rate fit*, which minimizes a global differential rate equation system to the complete, temperature-dependent data set. Haase *et al.* showed that extracting all relevant internal transition rates is possible by fitting the commonly assumed coupled differential equation system (7–8) to the data,²²

$$\dot{S}_1(t) = -(k_F + k_{ISC})S_1(t) + k_{RISC}T_1(t) \quad (7)$$

$$\dot{T}_1(t) = k_{ISC}S_1(t) - k_{RISC}T_1(t). \quad (8)$$

Here, k_F is the sum of radiative and nonradiative depopulation rates of the S_1 singlet state. The prerequisite for this model is the reduction of the TADF mechanism to a three-level system involving only S_0 , S_1 , T_1 .²⁰ This ignores the influence of disorder because in an organic molecule film, a broad distribution of states is present. Additionally, recombination from T_1 (nonradiative or as phosphorescence) is neglected, as well as a possible contribution from higher excited triplet states.²⁶ The influence of each of these simplifications will be explained in detail later.

The solution of equation system (7–8) equals the sum of two monoexponential functions with different amplitudes and rates, which is insufficient for modeling our data, which deviates from monoexponential decay especially during the PF. From the inverse Laplace transform analysis, we concluded that the non-monoexponential PF decay can be well described with two distinct rates in most cases. These decay characteristics are caused by dynamic and static inhomogeneities of the molecules' conformation and environment in film as discussed later in more detail.^{27,28} We assumed that k_F and k_{ISC} can

be treated as temperature-independent parameters because normalized PF decay showed no correlation with temperature. The advantage of fitting a rate equation system to the data, as demonstrated by Haase *et al.*, is the direct extraction of all internal rates. However, this evaluation method also consists of two steps: kinetic modeling and fitting of $k_{RISC}(T)$. We believe that a numerically more robust method is the direct extraction of all relevant parameters from the complete, temperature-dependent data set by global rate fitting in one step. We implemented an algorithm that includes the sum of two singlet states (as predicted by our Laplace evaluation which showed two distinct rate peaks of the fluorescence as shown in the SI). Both singlet states $S_{1,2}$ had a starting population of $N_{1,2}$ after excitation and were depopulated with rates $k_{F1,2}$, k_{ISC} and repopulated with k_{RISC} , depending on the triplet population $T_{1,2}(t)$, where $T_{1,2}(0) = 0$.

$$\dot{S}_{1,2}(t) = -(k_{F1,2} + k_{ISC})S_{1,2}(t) + k_{RISC}T_{1,2}(t) \quad (9)$$

$$\dot{T}_{1,2}(t) = k_{ISC}S_{1,2}(t) - k_{RISC}T_{1,2}(t) \quad (10)$$

$$k_{RISC} = k_A \exp\left(-\frac{\Delta E_{ST}}{k_B T}\right) \quad (11)$$

III. RESULTS AND DISCUSSION

Figure 3 shows the results of both evaluation methods for neat 4CzIPN and 3CzCIIPN films, respectively. Fit results are summarized in table 1. The Laplace fit algorithm fitted all data sets well on the full time scale of the decay while global rate fitting showed small deviations in the DF part of the decay after 1 μ s. We also tested more complex rate equation systems with multiple singlet and triplet states²⁶ in order to yield precise fits of the DF part, but found the process to be over-parameterized quickly, allowing very good fits but no robust way of extracting the effective values or possible distribution characteristics. This is shown and discussed in detail in the SI.

We now discuss the results for neat films and compare both evaluation methods with our calculated values and the literature. Both evaluation methods delivered matching values $\Delta E_{ST} = (54 \pm 5)$ meV for a neat 4CzIPN film. Depending on film matrix (or solvent), but also measurement technique and evaluation method, values between 30 meV and 140 meV are reported for 4CzIPN in the literature.^{6,26,29–34} However, in neat film with a similar experiment, Olivier *et al.* measured 42 meV (and simulated value: 60 meV), which is close to our result.³⁰ In 3CzCIIPN, we found $\Delta E_{ST} = (33 \pm 8)$ meV. Note, that this is the first value of ΔE_{ST} reported for 3CzCIIPN. The error in determining ΔE_{ST} increases for low ΔE_{ST} values because the temperature dependence of DF becomes small compared to the dynamic range of the complete decay. The mechanism behind the chlorine-induced decrease of ΔE_{ST} is explained later in the molecular

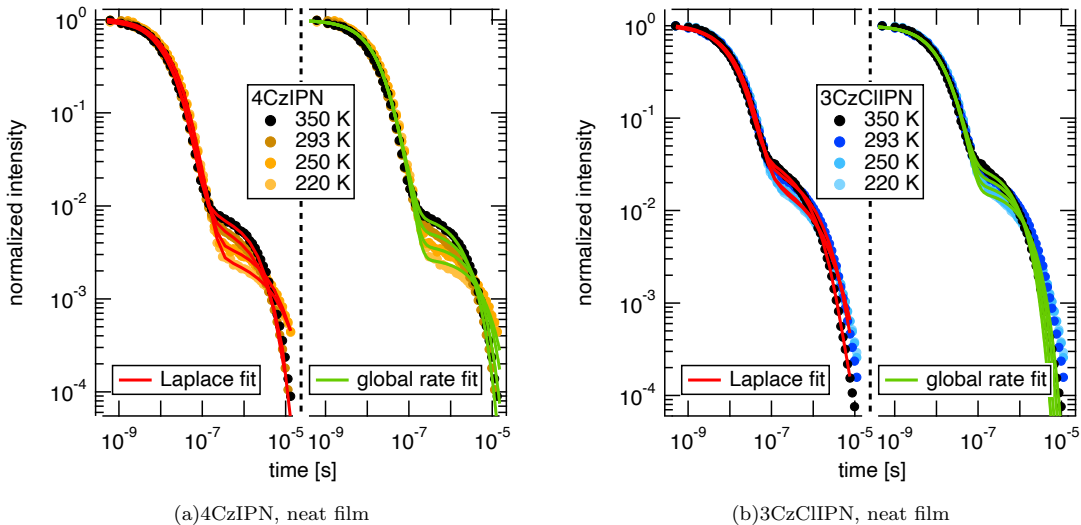


FIG. 3. Comparison of both fit methods applied to temperature-dependent transient fluorescence decay of neat TADF films

method	film	4CzIPN		3CzCIIPN	
		neat	in PS	neat	in PS
Laplace fit					
ΔE_{ST}	[meV]	54	65	34	38
k_{RISC}	$[10^6 \text{ s}^{-1}]$	0.6	0.7	2.1	1.8
k_A	$[10^6 \text{ s}^{-1}]$	5.1	8.7	7.6	8.9
$\langle \tau_{PF} \rangle$	[ns]	15	14	16	12
Global rate fit					
ΔE_{ST}	[meV]	54	62	33	30
$\langle k_F \rangle$	$[10^6 \text{ s}^{-1}]$	14	18	17	12
k_{RISC}	$[10^6 \text{ s}^{-1}]$	0.7	0.8	3.9	2.6
k_A	$[10^6 \text{ s}^{-1}]$	6.2	9.4	11	8.5
k_{ISC}	$[10^6 \text{ s}^{-1}]$	16	21	31	37
PLQY	[%]	n/a	99	n/a	54

TABLE I. Experimental results, k_{RISC} , $\langle k_F \rangle$ and $\langle \tau_{PF} \rangle$ at 293 K. PLQY for neat films was not measured due to strong reabsorption.

orbital calculation part. As explained in the introduction, internal transition rates are connected to the S_1 and T_1 energies as well as to their relative position. In the literature, k_{ISC} values between $(1 - 7) \cdot 10^7 \text{ s}^{-1}$ are reported.^{6,26,29-31,35,36} At room temperature, k_{RISC} values between $(6 - 12) \cdot 10^5 \text{ s}^{-1}$ are reported.^{6,30,31,36,37} Our results lie between these values (table I). With the global rate fit method, it is possible to simultaneously determine k_A and k_{ISC} . This is enabled by globally fitting for the optimized and temperature-independent k_{ISC} . Within our temperature range between 220 K and 350 K, we assume k_{ISC} to be constant.³⁵ As shown in table 1, the prefactor k_A was extracted with very good consistency by both evaluation methods. However, the global rate

fit revealed that the actual k_{ISC} is higher. Such results can also be found in the literature, when comparing published k_{ISC} values to the actual prefactor in the according $k_{RISC}(T)$ plots. The difference between k_{ISC} and k_A can be interpreted as intramolecular transition pathways which deviate from detailed balance, such as nonradiative losses³⁰, spin-orbit coupling²⁵, exciton diffusion²⁹ and dynamic asymmetries which result from internal reorganization of the excited charge transfer state. The absolute photoluminescence quantum yield (PLQY) of fluorophores (given by the ratio of emitted/absorbed photons, see SI for details) is dependent on a variety of parameters, such as molecular environment. To avoid reabsorption and fluorophore-fluorophore interaction, we measured the PLQY by embedding 1 wt% of TADF emitters in a PS matrix, a technique which is known from single molecule spectroscopy. Note, that the spectral characteristics of both, photoluminescence and electroluminescence spectra of 4CzIPN and 3CzCIIPN are similar, as shown in the SI. We measured a PLQY of $(99 \pm 1) \%$ for 4CzIPN and $(54 \pm 5) \%$ for 3CzCIIPN. Adachi *et al.* demonstrated that a reduction of the number of carbazole groups and change of substituents can decrease PLQY.⁶ The increased spin-orbit coupling caused by chlorine¹¹ may additionally introduce nonradiative transition pathways, thus lowering the PLQY. To examine how nonradiative depopulation of T_1 would affect the transients, we performed a global rate fit by adding a nonradiative pathway $T_1 \rightarrow S_0$ with rate (k_{nr}^T):

$$\dot{T}_1(t) = k_{ISC}S_1(t) - k_{RISC}T_1(t) - k_{nr}^T T_1(t). \quad (12)$$

This approach showed that high k_{nr}^T rates would lead to a faster DF decay than we experimentally observed. Therefore, $S_1 \rightarrow S_0$ is probably the main nonradiative

transition channel in 3CzClIPN. Compared to 4CzIPN, we also found a reduced PLQY of 3CzClIPN in solution (see SI).

To understand the molecular origin of the difference in ΔE_{ST} between 4CzIPN and 3CzClIPN, we performed quantum chemical calculations either based on density functional theory (DFT) or with Post-Hartree-Fock methods. A more detailed discussion of our calculations and in particular the results from regular time-dependent DFT (TD-DFT) calculations with and without Tamm-Dancoff approximation (TDA) can be found in the SI. Here, the focus of the presentation will be on the results from simplified TD-DFT (sTD-DFT) and simplified TDA (sTDA), which will be assessed *via* comparison with results from approximate coupled cluster singles and doubles (CC2) calculations with and without spin-component scaling (SCS), see table II.

method	4CzIPN			3CzClIPN		
	ΔE_{ST} [meV]	S_1 [eV]	T_1 [eV]	ΔE_{ST} [meV]	S_1 [eV]	T_1 [eV]
B3LYP						
sTD-DFT	46	2.411	2.365	41	2.341	2.300
sTDA	56	2.421	2.365	47	2.347	2.300
CAM-B3LYP						
sTD-DFT	77	3.056	2.979	49	3.013	2.964
sTDA	87	3.067	2.980	54	3.019	2.965
Post-HF						
CC2	43	2.842	2.798	22	2.847	2.824
SCS-CC2	38	3.179	3.140	16	3.204	3.188

TABLE II. Vertical singlet-triplet gaps and energies of the first excited singlet and triplet states relative to the optimized ground state.

The central quantity in our analysis is the energy difference between the S_1 and T_1 states for the ground state optimized geometries, *i.e.* the vertical ΔE_{ST} . For a more rigorous comparison with experiments, the energy difference of these two states in the corresponding minima should be determined, *i.e.* the adiabatic ΔE_{ST} .³⁸ Given the similarity of the two states for 4CzIPN and 3CzClIPN, we expect that the adiabatic singlet-triplet gap can be approximated by its vertical counterpart, which has been proposed by Penfold as well as by Tian *et al.*^{38,39} This is further corroborated by two theoretical studies of TADF molecules that reported similar trends for both definitions of ΔE_{ST} .^{40,41}

The unscaled CC2 calculations yield values for the vertical ΔE_{ST} that underestimate the experimental ones by *ca.* 10 meV. Nonetheless, the difference of this energy between the two compounds of 22 meV is close to its experimental counterpart. The application of SCS results in further lowering of both energies by around 5 meV, so the difference remains nearly constant. Overall, unscaled CC2 calculations to determine vertical ΔE_{ST} yield the best match with experiment among the employed meth-

ods (see the SI for a complete overview).

In case of the sTD-DFT/sTDA calculations, the results for individual ΔE_{ST} from sTD-DFT based on B3LYP ground state calculations are the closest to the CC2 reference. However, this property is only overestimated by 5 meV for 4CzIPN, whereas for 3CzClIPN the overestimation is 19 meV. Therefore, the difference in ΔE_{ST} is much too low with 5 meV. Employing sTDA leads to an increase of the S_1 energies, but hardly affects the T_1 energies. Owing to this, ΔE_{ST} increases and also their difference becomes slightly larger with 9 meV. Analyzing the results from sTD-DFT and sTDA calculations of ΔE_{ST} based on ground state calculations with the range-separated hybrid functional CAM-B3LYP, similar trends are found. However, the values for ΔE_{ST} are even higher than their B3LYP counterparts. Nonetheless, the sTD-DFT calculations with CAM-B3LYP functional yield a difference of 28 meV for ΔE_{ST} between the two compounds, which is the closest to the CC2 reference and experiment from all DFT-based calculations. Therefore, this approach appears promising for the investigation of trends in this property, whereas sTD-DFT calculations based on B3LYP ground state calculations might underestimate such changes. Overall, the semiempirical sTD-DFT and sTDA methods yield values for ΔE_{ST} that are much closer to the Post-Hartree-Fock calculations than the ones from regular TD-DFT and TDA calculations (see SI).

Insights into the nature of the S_1 and T_1 states can be obtained by visualizing the natural transition orbitals (NTOs), see figure 4. NTOs are compact orbital representations for the transition density resulting in a minimum number of electron-hole excitations.⁴² For all investigated electronic transitions, one pair of NTOs is dominant. These orbitals demonstrate that the S_1 and T_1 states are rather similar and there are also only small differences between the two compounds. The excited electron is mainly localized at the two cyano groups and the central benzene moiety. The hole is also found at the latter part, but it is also present at the carbazole units. It appears that the charge transfer character is more pronounced for 3CzClIPN than for 4CzIPN.

To quantify these findings, we performed wavefunction analysis and report the outcome for unscaled CC2 in the following. For this purpose, the molecules are divided into three fragments: the first one consists of the carbazole units, the second one of the benzene unit plus the chlorine atom in case of 3CzClIPN, and the third one of the cyano groups. Based on this fragmentation, we obtain similar values from wavefunction analysis for the S_1 and T_1 states of each compound. The charge transfer character can be used as a quantitative descriptor. It ranges from 0 for an excitation completely localized at one fragment to 1 for the case that electron and hole are localized at different fragments.⁴³ For 4CzIPN, this charge transfer character is 0.78 and 0.77 for S_1 and T_1 , respectively, and it increases to 0.84 and 0.83 for 3CzClIPN. Therefore, the increase in charge transfer

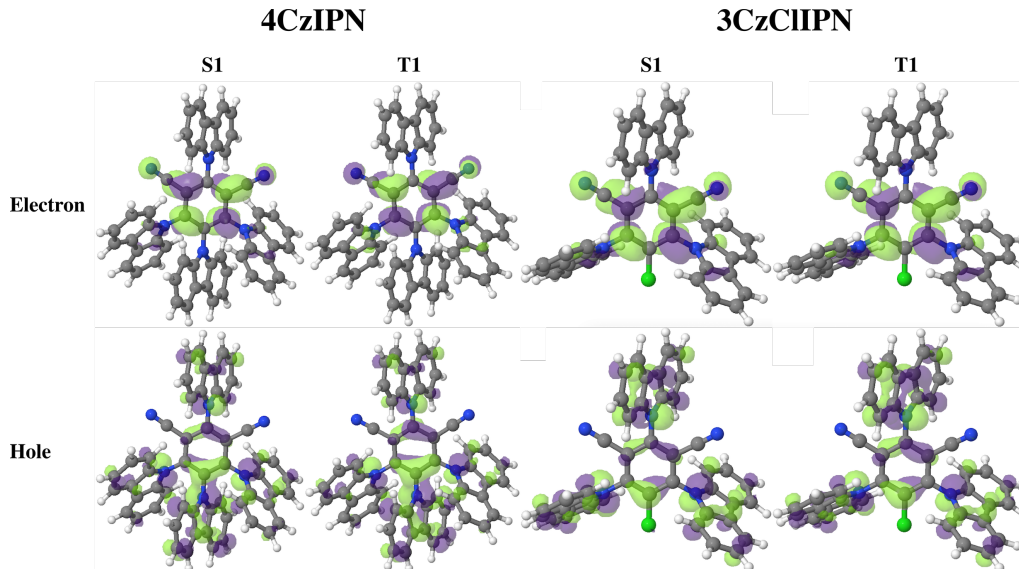


FIG. 4. Natural transition orbitals (NTO) of the first excited singlet state (S_1) and the first triplet state (T_1) from the CC2 calculations. For comparability, all NTOs are visualized with the same isovalue.

character leads to a decrease of ΔE_{ST} and further information on the performed wavefunction analysis along with the results for 3CzHIPN is given in the SI.

Next, we discuss the influence of the molecular environment in our measurements. Molecules which are sufficiently separated are known to show differences and fluctuations of their emission^{44,45} and absorption⁴⁶ spectra and lifetime.²⁸ This is caused by static differences of the molecular environment and dynamic variations of, for example, the side group movement and alignment of the molecule. The influence of the matrix (host) and molecular arrangement on TADF properties is widely discussed in the literature.^{25,30,34,37,47–52} To study the non-monoexponential decay characteristics of 4CzIPN and 3CzCIIPN in film, we compared neat films to PS films doped with a low (1 wt%) concentration of TADF molecules. Neat films of 4CzIPN and 3CzCIIPN show a strong red-shift and lower PLQY in comparison to doped PS films (see SI). This is mainly caused by selfabsorption (reabsorption within the film) and self-quenching.^{37,53} Polystyrene films doped with 1 wt% of 4CzIPN showed a slightly increased ΔE_{ST} compared to neat films. Considering the error of ± 8 meV, 3CzCIIPN shows similar results as neat film or embedded in PS. This indicates, that solid state solvation effects caused by matrix polarization and static charge transfer state stabilization⁴⁷ are minor when embedding 4CzIPN in PS, and negligible in case of 3CzCIIPN. This result is in agreement with a supplementary measurement by Olivier *et al.* who found similar decay characteristics of a neat 2CzPN (1,2-bis(carbazol-9-yl)-4,5-dicyanobenzene) film compared to a doped 98 wt% PS film.³⁰ We conclude that—although spectral properties are strongly affected by the matrix—the similar stretched exponential characteristics of the

transients are not only caused by static or dynamic film disorder, but by the molecules' large dihedral side group angles. This is in agreement with the work of Hasegawa *et al.* who found that the electronic states of 4CzIPN films are similar to the monomer.⁵⁰

IV. CONCLUSIONS

By investigating steady-state and time-dependent fluorescence characteristics, we elucidated the role of chlorine on the internal transition rates and singlet-triplet energy splitting ΔE_{ST} of 3CzCIIPN films compared to 4CzIPN. Although the photoluminescence and electroluminescence spectra of both materials is similar, quantum yield and temperature-dependent delayed fluorescence are drastically influenced by the chlorine group. Photoluminescence quantum yield was reduced by factor 2 in 3CzCIIPN, due to nonradiative transitions from the excited singlet to the ground state. Reverse intersystem crossing is strongly increased in 3CzCIIPN by factor 3–5 due to the lowered ΔE_{ST} . Quantum chemical calculations explained these findings by showing that chlorine increases the charge transfer character of the relevant states. This may also explain the increased photocatalytic efficiency of 3CzCIIPN in oxidations which was recently demonstrated.⁹ For potential applications of 3CzCIIPN in OLED devices, the nonradiative losses are a disadvantage. Our findings underline that precise knowledge of the excited states alone is insufficient in predicting the performance of a TADF molecule for potential applications in photocatalysis and OLED devices. To gain the necessary additional information about internal transition rates, we introduced a robust global evaluation

method for transient fluorescence data which outputs all parameters of the specified TADF model in one single optimization step. By comparing neat films to diluted polystyrene films, we concluded that the often observed stretched exponential transient characteristics of TADF materials are a feature of large dihedral side group angles in condensed phase.

V. METHODS

All decay data sets and fit functions were normalized in order to reduce optimization parameters. The algorithm then minimized the global difference between temperature-dependent data and the solution of the temperature-dependent rate equations. The global difference vector was weighted with a three part step function, emphasizing the 1 – 5 μ s part of the decay, where DF is measured with the best signal-to-noise ratio. All fit parameters (N_1 , N_2 , k_F^1 , k_F^2 , k_{ISC} , k_A , ΔE_{ST}) are global. TADF and TADF:polystyrene (PS) films were prepared by spincoating. Silicon substrates with 100 nm of thermally grown oxide were used. Substrates and glassware were cleaned by annealing at 450° C for two hours in a laboratory oven. PS with a molar mass of 20 kg mol⁻¹ was doped with 1 wt% of 4CzIPN and 3CzClIPN, respectively, at a total concentration of 10 mg ml⁻¹. For neat dye films, 0.1 mg ml⁻¹ of dye in toluene was used. The samples were measured with a homebuilt laser scan confocal microscope in a cryostate (Janis, ST500) with a Zeiss LWD 63 \times , NA=0.75 objective. Fluorescence decay was acquired with time-correlated single photon counting (TCSPC) using a Perkin Elmer avalanche photodiode (APD) and a PicoHarp300 TCSPC module (PicoQuant). The PicoHarp300 was set to the maximum time window of 33.55 μ s with a time resolution of 0.512 ns per channel. Data was logarithmically binned and the background level subtracted. The samples were excited with a 465 nm pulsed diode laser (PicoQuant, $\tau_{IRF} < 1$ ns) at a repetition rate of 25 kHz. Fluorescence was detected with a 500 nm longpass filter. Each decay curve was measured by integrating for 15 minutes. The dark count rate of the APD was 50 cts (counts per second). The objective was defocussed until the fluorescence signal was below 1000 cts on the APD to ensure falling below the general 5% limit of the TCSPC technique (signal photons to laser pulses per time interval).⁵⁴ This condition avoids pile-up effects caused by the total dead time of the TCSPC system. Although the dark count to signal ratio suggests a signal to noise ratio of only 10:1, the effective ratio is better than 10000:1 because 1000 cts of signal refer to the decay occurring within few microseconds while the dark count rate refers to one second. We want to emphasize that measuring time-dependent fluorescence in both, nanosecond and microsecond (or millisecond) time regimes with equal experimental parameters is challenging and demands ensuring appropriate equilibrium conditions of optical excitation and decay.

Measuring at non-equilibrium conditions leads to wrong results and conclusions. This is especially the case at low temperatures, materials with long DF lifetimes and when measuring PF and DF separately with different excitation sources (or laser repetition rates) on different time scales.

ACKNOWLEDGMENTS

C. W. acknowledges funding by the German Research Foundation (DFG) via a return fellowship (reference number: WI 4853/2-1). The quantum chemical calculations were performed on resources provided by the Leipzig University Computing Centre and by the Paderborn Center for Parallel Computing. C. W. also thanks Stefan Zahn, Bernd Abel, and Jörg Matysik for discussions and support.

CORRESPONDING AUTHOR

Email: deibel@physik.tu-chemnitz.de

NOTES

The authors declare no competing financial interest.

SUPPLEMENTARY INFORMATION

Inverse Laplace fit results, additional rate model fit results, global rate fit results, $k_{RISC}(T)$ plots, simulation results, UV-Vis spectra, quantum yield, streak measurements, quantum chemical calculations

REFERENCES

- ¹ Hung, L.; Chen, C. Recent Progress of Molecular Organic Electroluminescent Materials and Devices. *Mater. Sci. Eng. R Rep* **2002**, *39*, 143–222.
- ² Reineke, S.; Lindner, F.; Schwartz, G.; Seidler, N.; Walzer, K.; Lüssem, B.; Leo, K. White Organic Light-emitting Diodes with Fluorescent Tube Efficiency. *Nature* **2009**, *459*, 234.
- ³ Sun, Y.; Giebink, N. C.; Kanno, H.; Ma, B.; Thompson, M. E.; Forrest, S. R. Management of Singlet and Triplet Excitons for Efficient White Organic Light-emitting Devices. *Nature* **2006**, *440*, 908.
- ⁴ Zeitler, K. Photoredox Catalysis with Visible Light. *Angew. Chem. Int. Ed.* **2009**, *48*, 9785–9789.
- ⁵ Adachi, C.; Baldo, M. A.; Thompson, M. E.; Forrest, S. R. Nearly 100% Internal Phosphorescence Efficiency in an Organic Light-emitting Device. *J. Appl. Phys.* **2001**, *90*, 5048–5051.
- ⁶ Uoyama, H.; Goushi, K.; Shizu, K.; Nomura, H.; Adachi, C. Highly Efficient Organic Light-emitting Diodes from Delayed Fluorescence. *Nature* **2012**, *492*, 234.
- ⁷ Onsager, L. Reciprocal Relations in Irreversible Processes. I. *Phys. Rev.* **1931**, *37*, 405.
- ⁸ Hirata, S.; Sakai, Y.; Masui, K.; Tanaka, H.; Lee, S. Y.; Nomura, H.; Nakamura, N.; Yasumatsu, M.; Nakanotani, H.; Zhang, Q., et al. Highly Efficient Blue Electroluminescence Based on Thermally Activated Delayed Fluorescence. *Nat. Mater.* **2015**, *14*, 330.
- ⁹ Speckmeier, E.; Fischer, T. G.; Zeitler, K. A Toolbox Approach To Construct Broadly Applicable Metal-Free Catalysts for Photoredox Chemistry: Deliberate Tuning of Redox Potentials and Importance of Halogens in Donor–Acceptor Cyanoarenes. *J. Am. Chem. Soc.* **2018**, *140*, 15353–15365.
- ¹⁰ Lowry, M. S.; Goldsmith, J. I.; Slinker, J. D.; Rohl, R.; Pascal, R. A.; Malliaras, G. G.; Bernhard, S. Single-layer Electroluminescent Devices and Photoinduced Hydrogen Production from an Ionic Iridium (III) Complex. *Chem. Mater.* **2005**, *17*, 5712–5719.
- ¹¹ Xiang, Y.; Zhao, Y.; Xu, N.; Gong, S.; Ni, F.; Wu, K.; Luo, J.; Xie, G.; Lu, Z.-H.; Yang, C. Halogen-induced Internal Heavy-atom Effect Shortening the Emissive Lifetime and Improving the Fluorescence Efficiency of Thermally Activated Delayed Fluorescence Emitters. *J. Mater. Chem. C* **2017**, *5*, 12204–12210.
- ¹² Kretzschmar, A.; Patze, C.; Schwaebel, S. T.; Bunz, U. H. Development of Thermally Activated Delayed Fluorescence Materials with Shortened Emissive Lifetimes. *J. Org. Chem.* **2015**, *80*, 9126–9131.
- ¹³ Dias, F. B.; Bourdakos, K. N.; Jankus, V.; Moss, K. C.; Kamtekar, K. T.; Bhalla, V.; Santos, J.; Bryce, M. R.; Monkman, A. P. Triplet Harvesting with 100% Efficiency by Way of Thermally Activated Delayed Fluorescence in Charge Transfer OLED Emitters. *Adv. Mater.* **2013**, *25*, 3707–3714.
- ¹⁴ Dias, F. B.; Penfold, T. J.; Monkman, A. P. Photophysics of Thermally Activated Delayed Fluorescence Molecules. *Methods Appl. Fluoresc.* **2017**, *5*, 012001.
- ¹⁵ Zhang, Q.; Li, B.; Huang, S.; Nomura, H.; Tanaka, H.; Adachi, C. Efficient Blue Organic Light-emitting Diodes Employing Thermally Activated Delayed Fluorescence. *Nat. Photonics* **2014**, *8*, 326.
- ¹⁶ Gibson, J.; Monkman, A. P.; Penfold, T. J. The Importance of Vibronic Coupling for Efficient Reverse Intersystem Crossing in Thermally Activated Delayed Fluorescence Molecules. *ChemPhysChem* **2016**, *17*, 2956–2961.
- ¹⁷ Zhang, Q.; Li, J.; Shizu, K.; Huang, S.; Hirata, S.; Miyazaki, H.; Adachi, C. Design of Efficient Thermally Activated Delayed Fluorescence Materials for Pure Blue Organic Light Emitting Diodes. *J. Am. Chem. Soc.* **2012**, *134*, 14706–14709.
- ¹⁸ Berberan-Santos, M. N.; Garcia, J. M. Unusually Strong Delayed Fluorescence of C70. *J. Am. Chem. Soc.* **1996**, *118*, 9391–9394.
- ¹⁹ Baleizão, C.; Berberan-Santos, M. N. Thermally Activated Delayed Fluorescence as a Cycling Process between Excited Singlet and Triplet States: Application to the Fullerenes. *J. Chem. Phys.* **2007**, *126*, 204510.
- ²⁰ Penfold, T.; Dias, F.; Monkman, A. The Theory of Thermally Activated Delayed Fluorescence for Organic Light Emitting Diodes. *ChemComm* **2018**, *54*, 3926–3935.
- ²¹ Scholz, R.; Kleine, P.; Lygaitis, R.; Popp, L.; Lenk, S.; Etherington, M. K.; Monkman, A. P.; Reineke, S. Investigation of Thermally Activated Delayed Fluorescence from a Donor–Acceptor Compound with Time-Resolved Fluorescence and Density Functional Theory Applying an Optimally Tuned Range-Separated Hybrid Functional. *J. Phys. Chem. A* **2020**, *124*, 1535–1553.
- ²² Haase, N.; Danos, A.; Pflumm, C.; Morherr, A.; Stachelek, P.; Mekić, A.; Brütting, W.; Monkman, A. P. Kinetic Modeling of Transient Photoluminescence from Thermally Activated Delayed Fluorescence. *J. Phys. Chem. C* **2018**, *122*, 29173–29179.
- ²³ Reichert, S.; Flemming, J.; An, Q.; Vaynzof, Y.; Pietschmann, J.-F.; Deibel, C. Ionic-Defect Distribution Revealed by Improved Evaluation of Deep-Level Transient Spectroscopy on Perovskite Solar Cells. *Phys. Rev. Appl.* **2020**, *13*, 034018.
- ²⁴ Lakowicz, J. R. *Principles of Fluorescence Spectroscopy*; Springer Science & Business Media, 2013.
- ²⁵ Hosokai, T.; Nakanotani, H.; Santou, S.; Noda, H.; Nakayama, Y.; Adachi, C. TADF Activation by Solvent Freezing: The Role of Nonradiative Triplet Decay and Spin-orbit Coupling in Carbazole Benzonitrile Derivatives. *Synth. Met.* **2019**, *252*, 62–68.
- ²⁶ Kobayashi, T.; Niwa, A.; Takaki, K.; Haseyama, S.; Nagase, T.; Goushi, K.; Adachi, C.; Naito, H. Contributions of a Higher Triplet Excited State to the Emission Properties of a Thermally Activated Delayed Fluorescence Emitter. *Phys. Rev. Appl.* **2017**, *7*, 034002.
- ²⁷ Noriega, R.; Barnard, E. S.; Ursprung, B.; Cotts, B. L.; Penwell, S. B.; Schuck, P. J.; Ginsberg, N. S. Uncovering Single-molecule Photophysical Heterogeneity of Bright, Thermally Activated Delayed Fluorescence Emitters Dispersed in Glassy Hosts. *J. Am. Chem. Soc.* **2016**, *138*,

- 13551–13560.
- ²⁸ Börner, R.; Kowerko, D.; Krause, S.; Borczyskowski, C. v.; Hübner, C. G. Efficient Simultaneous Fluorescence Orientation, Spectrum, and Lifetime Detection for Single Molecule Dynamics. *J. Chem. Phys.* **2012**, *137*, 164202.
- ²⁹ Yurash, B.; Nakanotani, H.; Olivier, Y.; Beljonne, D.; Adachi, C.; Nguyen, T.-Q. Photoluminescence Quenching Probes Spin Conversion and Exciton Dynamics in Thermally Activated Delayed Fluorescence Materials. *Adv. Mater.* **2019**, *31*, 1804490.
- ³⁰ Olivier, Y.; Yurash, B.; Muccioli, L.; D’Avino, G.; Mikhnenko, O.; Sancho-Garcia, J.-C.; Adachi, C.; Nguyen, T.-Q.; Beljonne, D. Nature of the Singlet and Triplet Excitations Mediating Thermally Activated Delayed Fluorescence. *Phys. Rev. Mater.* **2017**, *1*, 075602.
- ³¹ Noda, H.; Chen, X.-K.; Nakanotani, H.; Hosokai, T.; Miyajima, M.; Notsuka, N.; Kashima, Y.; Brédas, J.-L.; Adachi, C. Critical Role of Intermediate Electronic States for Spin-flip Processes in Charge-transfer-type Organic Molecules with Multiple Donors and Acceptors. *Nat. Mater.* **2019**, *18*, 1084–1090.
- ³² Menke, S. M.; Holmes, R. J. Exciton Transport in an Organic Semiconductor Exhibiting Thermally Activated Delayed Fluorescence. *J. Phys. Chem. C* **2016**, *120*, 8502–8508.
- ³³ Niwa, A.; Kobayashi, T.; Nagase, T.; Goushi, K.; Adachi, C.; Naito, H. Temperature Dependence of Photoluminescence Properties in a Thermally Activated Delayed Fluorescence Emitter. *Appl. Phys. Lett.* **2014**, *104*, 79.1.
- ³⁴ Ishimatsu, R.; Matsunami, S.; Shizu, K.; Adachi, C.; Nakano, K.; Imato, T. Solvent Effect on Thermally Activated Delayed Fluorescence by 1, 2, 3, 5-tetrakis (carbazol-9-yl)-4, 6-dicyanobenzene. *J. Phys. Chem. A* **2013**, *117*, 5607–5612.
- ³⁵ Kobayashi, T.; Kawate, D.; Niwa, A.; Nagase, T.; Goushi, K.; Adachi, C.; Naito, H. Intersystem Crossing Rate in Thermally Activated Delayed Fluorescence Emitters. *Phys. Status Solidi A* **2019**,
- ³⁶ Einzinger, M.; Zhu, T.; de Silva, P.; Belger, C.; Swager, T. M.; Van Voorhis, T.; Baldo, M. A. Shorter Exciton Lifetimes via an External Heavy-Atom Effect: Alleviating the Effects of Bimolecular Processes in Organic Light-Emitting Diodes. *Adv. Mater.* **2017**, *29*, 1701987.
- ³⁷ Kim, H. S.; Park, S.-R.; Suh, M. C. Concentration Quenching Behavior of Thermally Activated Delayed Fluorescence in a Solid Film. *J. Phys. Chem. C* **2017**, *121*, 13986–13997.
- ³⁸ Penfold, T. J. On Predicting the Excited-State Properties of Thermally Activated Delayed Fluorescence Emitters. *J. Phys. Chem. C* **2015**, *119*, 13535–13544.
- ³⁹ Theoretical Predication for Transition Energies of Thermally Activated Delayed Fluorescence Molecules. *Chin. Chem. Lett.* **2016**, *27*, 1445–1452.
- ⁴⁰ Sun, H.; Zhong, C.; Brédas, J.-L. Reliable Prediction with Tuned Range-Separated Functionals of the Singlet–Triplet Gap in Organic Emitters for Thermally Activated Delayed Fluorescence. *J. Chem. Theory Comput.* **2015**, *11*, 3851–3858.
- ⁴¹ Olivier, Y.; Moral, M.; Muccioli, L.; Sancho-García, J.-C. Dynamic Nature of Excited States of Donor–acceptor TADF Materials for OLEDs: How Theory can Reveal Structure–property Relationships. *J. Mater. Chem. C* **2017**, *5*, 5718–5729.
- ⁴² Martin, R. L. Natural Transition Orbitals. *J. Chem. Phys.* **2003**, *118*, 4775–4777.
- ⁴³ Plasser, F.; Lischka, H. Analysis of Excitonic and Charge Transfer Interactions from Quantum Chemical Calculations. *J. Chem. Theory Comput.* **2012**, *8*, 2777–2789.
- ⁴⁴ Ambrose, W.; Moerner, W. Fluorescence Spectroscopy and Spectral Diffusion of Single Impurity Molecules in a Crystal. *Nature* **1991**, *349*, 225.
- ⁴⁵ Krause, S.; Kowerko, D.; Börner, R.; Hübner, C. G.; von Borczyskowski, C. Spectral Diffusion of Single Molecules in a Hierarchical Energy Landscape. *ChemPhysChem* **2011**, *12*, 303–312.
- ⁴⁶ Streiter, M.; Krause, S.; von Borczyskowski, C.; Deibel, C. Dynamics of Single-molecule Stokes Shifts: Influence of Conformation and Environment. *J. Phys. Chem. Lett.* **2016**, *7*, 4281–4284.
- ⁴⁷ Northey, T.; Stacey, J.; Penfold, T. The Role of Solid State Solvation on the Charge Transfer State of a Thermally Activated Delayed Fluorescence Emitter. *J. Mater. Chem. C* **2017**, *5*, 11001–11009.
- ⁴⁸ Cho, Y. J.; Yook, K. S.; Lee, J. Y. High Efficiency in a Solution-processed Thermally Activated Delayed-fluorescence Device Using a Delayed-fluorescence Emitting Material with Improved Solubility. *Adv. Mater.* **2014**, *26*, 6642–6646.
- ⁴⁹ Mamada, M.; Inada, K.; Komino, T.; Potscavage Jr, W. J.; Nakanotani, H.; Adachi, C. Highly Efficient Thermally Activated Delayed Fluorescence from an Excited-state Intramolecular Proton Transfer System. *ACS Cent. Sci.* **2017**, *3*, 769–777.
- ⁵⁰ Hasegawa, Y.; Yamada, Y.; Sasaki, M.; Hosokai, T.; Nakanotani, H.; Adachi, C. Well-ordered 4CzIPN ((4s, 6s)-2, 4, 5, 6-Tetra (9-H-carbazol-9-yl) isophthalonitrile) Layers: Molecular Orientation, Electronic Structure, and Angular Distribution of Photoluminescence. *J. Phys. Chem. Lett.* **2018**, *9*, 863–867.
- ⁵¹ Cucchi, M.; Matulaitis, T.; Kukhta, N. A.; Grazulevicius, J. V.; Reineke, S.; Scholz, R. Influence of the Dielectric Constant Around an Emitter on its Delayed Fluorescence. *Phys. Rev. Appl.* **2019**, *12*, 044021.
- ⁵² Takeda, H.; Takeda, M.; Yoshioka, H.; Minamide, H.; Oki, Y.; Adachi, C. Fluorescence Lifetime Elongation of Thermally Activated Delayed Fluorescence 4CzIPN Molecules with Encapsulation into Zeolitic Imidazole Frameworks ZIF-11. *Opt. Mater. Express* **2019**, *9*, 1150–1160.
- ⁵³ Ahn, T.-S.; Al-Kaysi, R. O.; Müller, A. M.; Wentz, K. M.; Bardeen, C. J. Self-absorption Correction for Solid-state Photoluminescence Quantum Yields Obtained from Integrating Sphere Measurements. *Rev. Sci. Instrum.* **2007**, *78*, 086105.
- ⁵⁴ Becker, W. *The bh TCSPC handbook*; Becker & Hickl, 2014.

Supporting Information

Impact of chlorine on the internal transition rates and excited states of the thermally delayed activated fluorescence molecule 3CzClIPN

Martin Streiter,¹ Tillmann Fischer,² Christian Wiebeler,^{3,4} Sebastian Reichert,¹ Jörn Langenickel,⁵ Kirsten Zeitler,² and Carsten Deibel¹

¹*Institut für Physik, Technische Universität Chemnitz, 09126 Chemnitz, Germany*

²*Institut für Organische Chemie, Universität Leipzig, 04103 Leipzig, Germany*

³*Institut für Analytische Chemie, Universität Leipzig, 04103 Leipzig, Germany*

⁴*Leibniz-Institut für Oberflächenmodifizierung (IOM), 04318 Leipzig, Germany*

⁵*Zentrum für Mikrotechnologien, Technische Universität Chemnitz, 09126 Chemnitz, Germany*

I. EQUATIONS

Effective rate k_{DF} :

$$\langle k_{DF} \rangle = \frac{A_1 k_{DF1}^{-1} + A_2 k_{DF1}^{-1}}{A_1 k_{DF1}^{-2} + A_2 k_{DF2}^{-2}} \quad (1)$$

Effective photoluminescence rate determined with amplitude-weighted rates k_F :

$$\langle k_F \rangle = \frac{A_1 k_{F1}^{-1} + A_2 k_{F1}^{-1}}{A_1 k_{F1}^{-2} + A_2 k_{F2}^{-2}} \quad (2)$$

Effective photoluminescence lifetime determined with the two main amplitude-weighted exponential rates from inverse Laplace transform:

$$\langle \tau_{PL} \rangle = \frac{A_1 k_{F1}^{-2} + A_2 k_{F2}^{-2}}{A_1 k_{F1}^{-1} + A_2 k_{F1}^{-1}} \quad (3)$$

II. LAPLACE TRANSFORM FIT

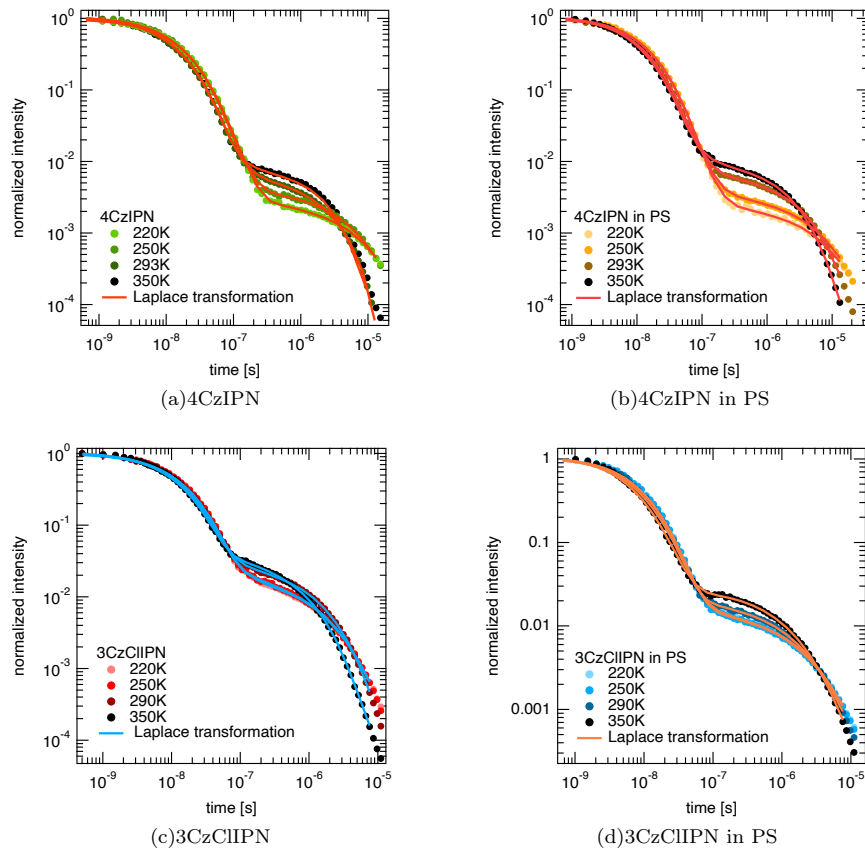


FIG. 1: Laplace transform fits

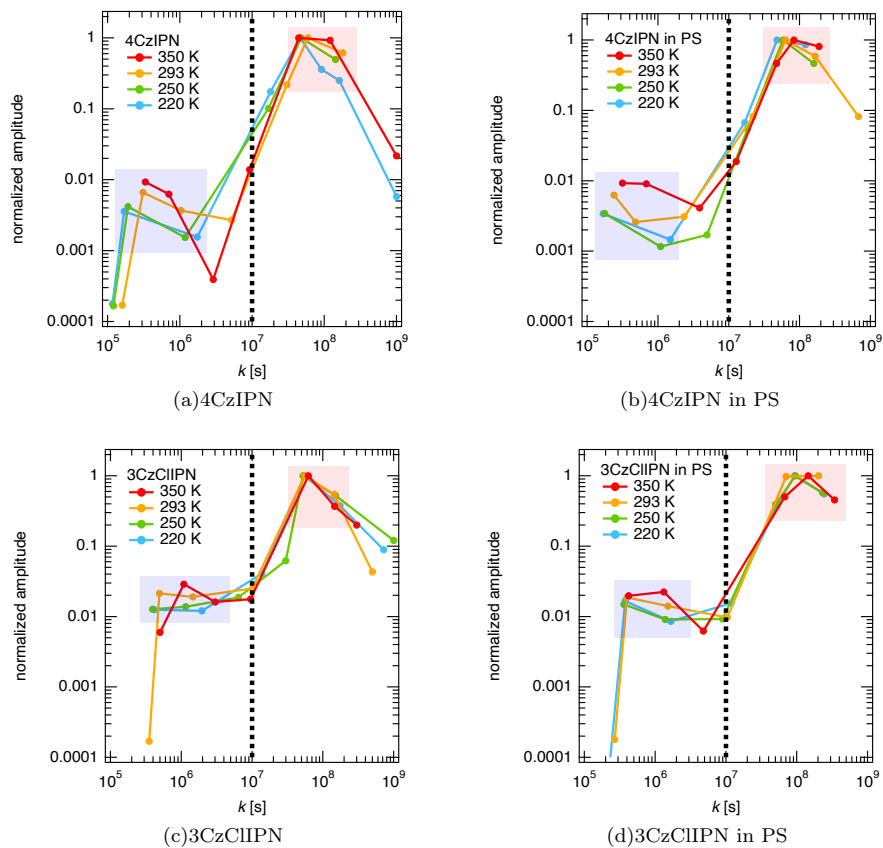


FIG. 2: Laplace rates and amplitudes

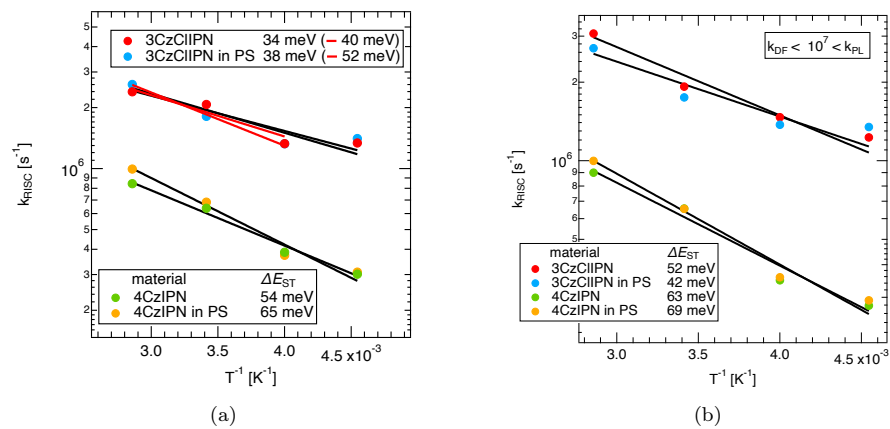


FIG. 3: Arrhenius plots of Laplace analysis

III. ALTERNATIVE RATE DIFFERENTIAL EQUATION FITS

It is possible to achieve precise fits which fit the stretched exponential part of the delayed fluorescence by summing up two singlet states $S_1(t) + S_2(t)$. Both $S(t)$ functions are the solution of the following coupled differential equation system with individual depopulation rates k_F , reverse intersystem crossing rates k_{RISC} and one shared intersystem crossing rate k_{ISC} :

$$\dot{S}_1(t) = -(k_{F1} + k_{\text{ISC}})S_1(t) + k_{\text{RISC}1}T_1(t) \quad (4)$$

$$\dot{T}_1(t) = k_{\text{ISC}}S_1(t) - k_{\text{RISC}1}T_1(t) \quad (5)$$

$$\dot{S}_2(t) = -(k_{F2} + k_{\text{ISC}})S_2(t) + k_{\text{RISC}2}T_2(t) \quad (6)$$

$$\dot{T}_2(t) = k_{\text{ISC}}S_2(t) - k_{\text{RISC}2}T_2(t). \quad (7)$$

A. Fits

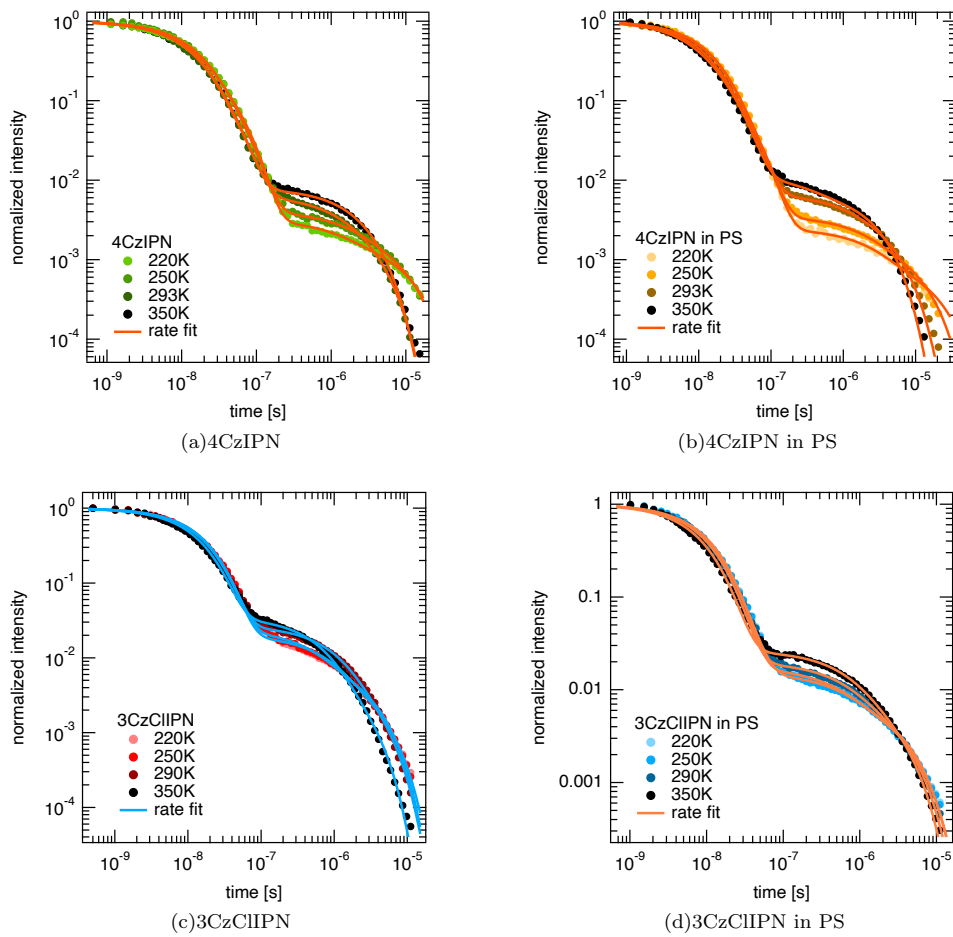


FIG. 4: Distribution of k_{RISC}

B. Rate analysis

Assuming two different ΔE_{ST} was suggested by Kobayashi *et al.* for neat 4CzIPN films.¹ However, it is not clear if interpreting the Arrhenius plot is useful for two different k_{RISC} (or the corresponding weighted Arithmetic or geometric means as shown in figures B a-d) because they are not connected. Therefore, the deviation between both k_{RISC} looks differently for each sample, although all fits have a similar quality. This also makes treating the approach as a global fit difficult. Interpreting the temperature-dependent k_{RISC}^1 and k_{RISC}^2 individually leads to values which are not plausible. The geometric mean deviates from the values presented in the main paper without a clear trend. All Arrhenius fits with $k_{RISC} = k_A \exp(-\Delta E_{ST}/k_B T)$ are summarized in table I.

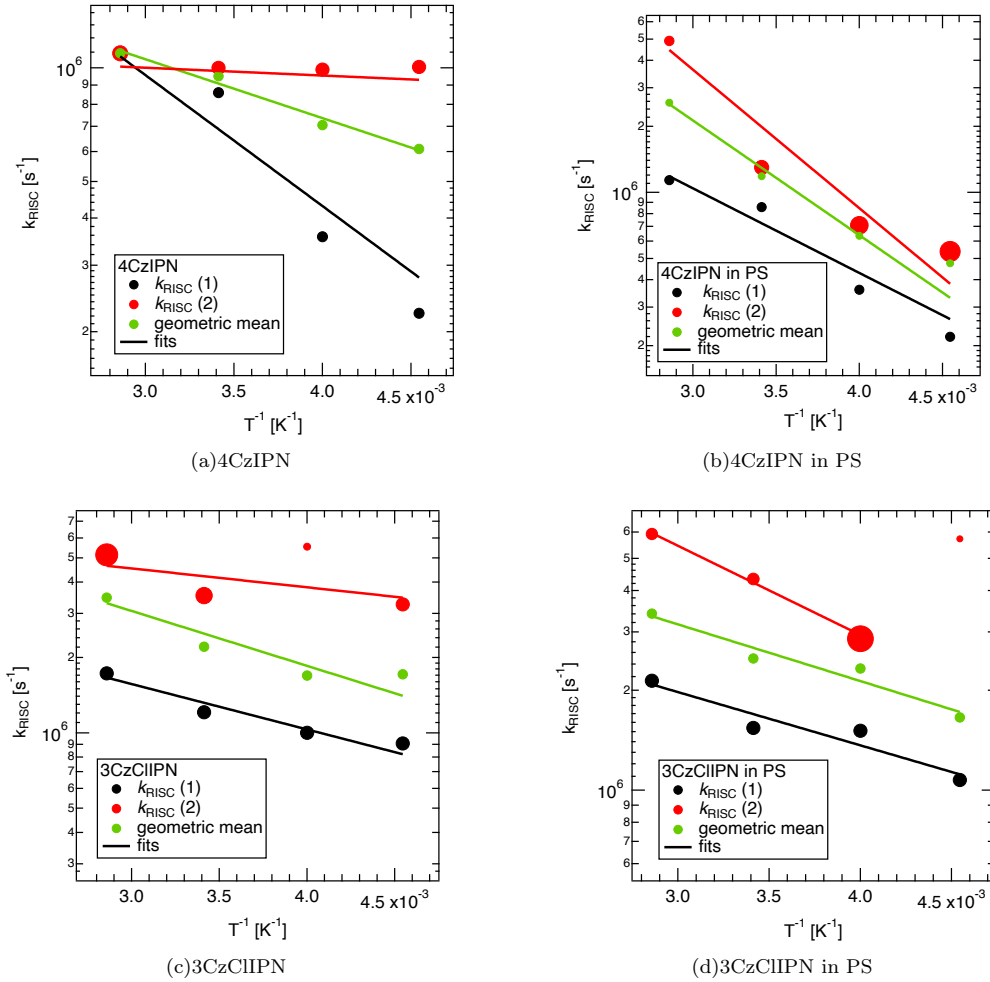


FIG. 5: Weighted (dot size) k_{RISC} rates from rate fits.

		4CzIPN		3CzCIIPN	
		neat film	in PS	neat film	in PS
$\Delta E_{ST}(1)$	[meV]	69	76	36	32
$\Delta E_{ST}(2)$	[meV]	4	125	15	53
$\Delta E_{ST}(\text{geo})$	[meV]	31	104	43	34

TABLE I: Individual ΔE_{ST} and weighted geometric means of the Arrhenius plots.

IV. GLOBAL FITS

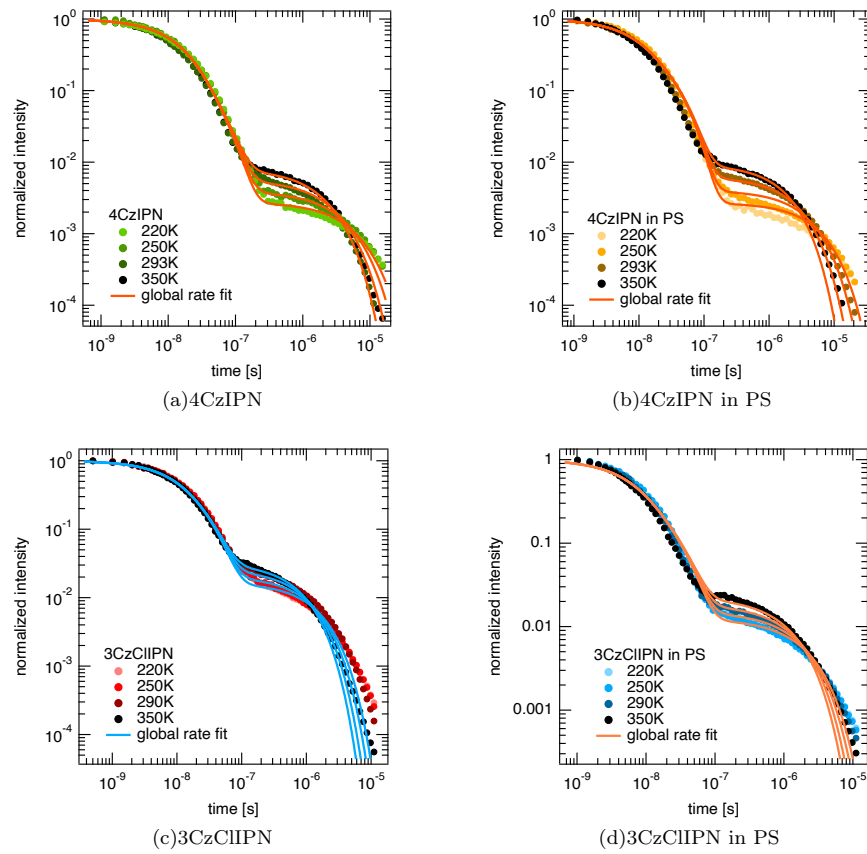


FIG. 6: global fits

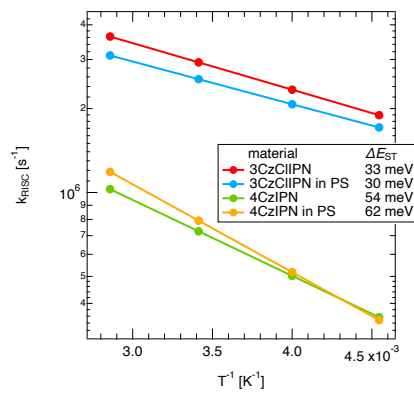


FIG. 7: Arrhenius plot of global fits

V. STEADY-STATE MEASUREMENTS

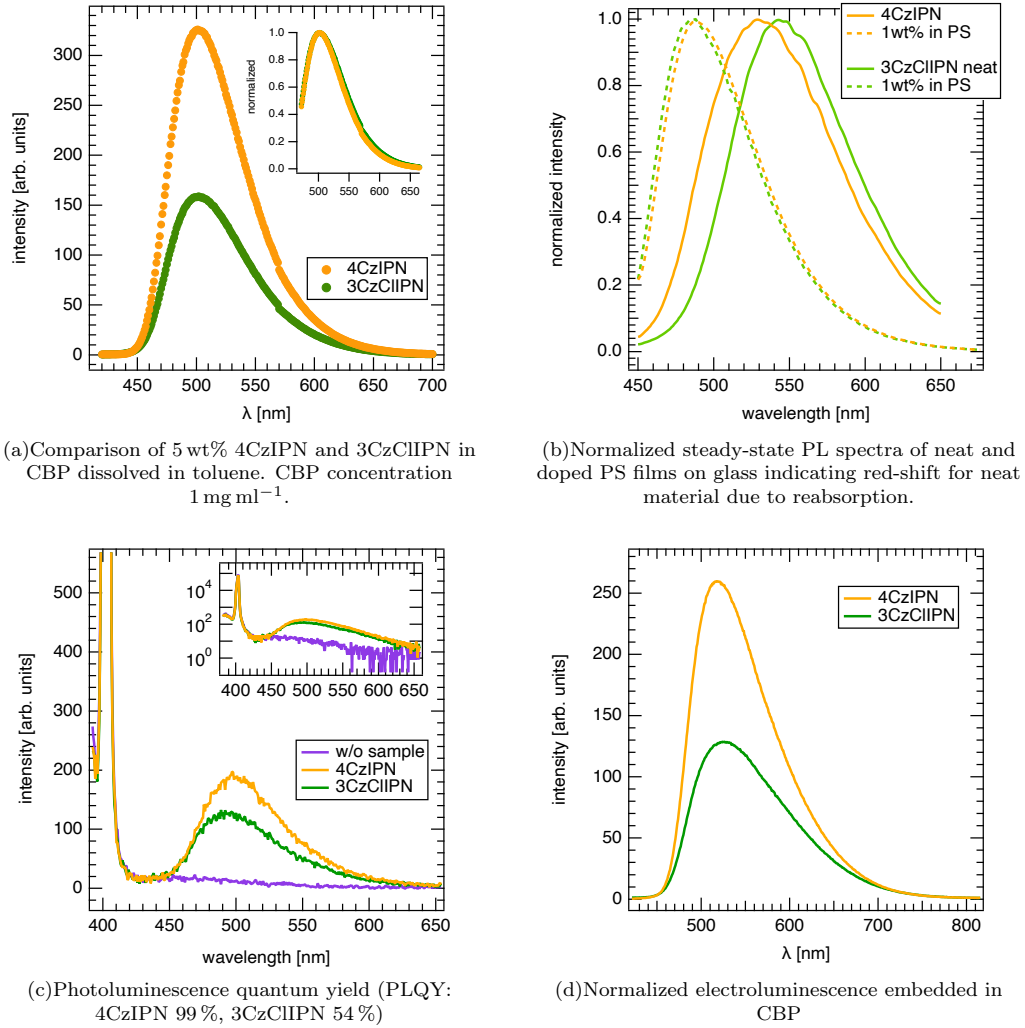


FIG. 8: Steady-state spectra

Spectra of 4CzIPN and 3CzCIIPN in solution and as films were measured with a Cary Eclipse spectrometer (Varian) and excited at 405 nm. The absolute photoluminescence quantum yield (PLQY) was determined by measuring the spectrum (OceanOptics, QE pro - calibrated with an ORIEL 63358 tungsten lamp) of the excitation laser diode (Thorlabs, 405 nm) and the 1 wt% 4CzIPN (3CzCIIPN) on glass film simultaneously. As a reference, a clean glass substrate was measured. PLQY is then calculated with $(\text{emitted PL})/(\text{laser signal from clean glass} - \text{laser signal from TADF sample})$. For the measurement of electroluminescence, structured ITO substrates were spincoated with ZnO-NP (zinc oxide nanoparticles) dissolved in ethanol (50 mg ml^{-1} at 2000 rpm) and 5 wt% of 4CzIPN (3CzCIIPN) in CBP (4,4'-Bis(*N*-carbazolyl)-1,1'-biphenyl) dissolved in toluene (12 mg ml^{-1} at 1500 rpm). These films then were subsequently evaporated with 40 nm HMTPD (*N,N,N',N'*-Tetrakis(3-methylphenyl)-3,3'-dimethylbenzidine), 10 nm molybdenum oxide and 100 nm aluminum. A voltage of 6 V was applied and the spectrum was measured with a 200 μm , NA 0.22 fiber which was coupled to the substrate and the spectrometer (OceanOptics, QE pro).

VI. TIME-RESOLVED MEASUREMENTS

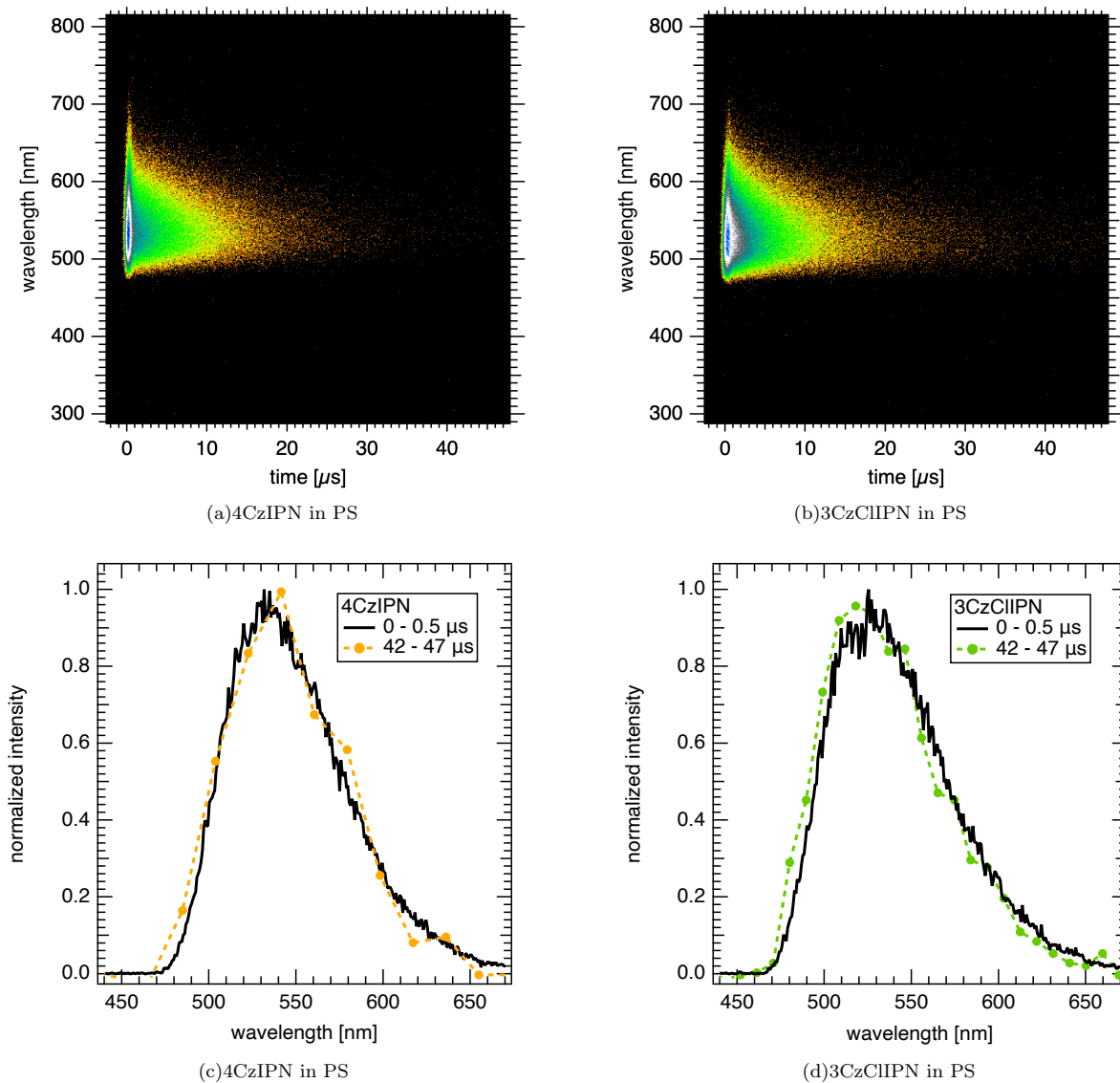


FIG. 9: Time-resolved spectra

Streak measurements were performed on a Hamamatsu C10910-05 camera. Films were excited at 405 nm with a pulse rate of 10 kHz (Light Conversion, Pharos laser with Orpheus OPA) in an evacuated cryostat (JANIS, ST-500). Delayed spectra were binned to 12 data points. Note, that the PL part of the decay is distorted when measuring the full decay in a 50 μ s window, as the IRF is longer than the nanosecond decay. To evaluate transients, the PL must be additionally measured in a smaller time window (50–200 ns) at the same pulse rate.

VII. QUANTUM CHEMICAL CALCULATIONS

Structural models of 4CzIPN and 3CzIPN were generated with GaussView.² Their ground state geometries were optimized with density functional theory (DFT) calculations utilizing the B3LYP functional,³⁻⁵ which has been applied in previous studies of TADF emitter materials.⁶⁻¹² Furthermore, Grimme dispersion correction with Becke-Johnson damping (D3BJ)^{13,14} was employed to improve the description of the interaction between the carbazole units.^{15,16} During the optimizations, the double- ζ Pople style basis set 6-31+G* was utilized.¹⁷ Calculations of vibrational frequencies on the same level of theory were realized to check that the optimized structures correspond to minima on the potential energy surface. The subsequent time-dependent DFT (TD-DFT) calculations with and without Tamm-Dancoff approximation (TDA) for the first 20 excited states with singlet and triplet multiplicity were performed with the same basis set employing either the B3LYP functional as for the structure optimizations or the range-separated hybrid functional CAM-B3LYP.¹⁸ The described quantum chemical calculations were realized with the Gaussian 16 software package.¹⁹

Furthermore, the Orca program^{20,21} was used for the sTD-DFT and sTDA calculations²²⁻²⁴ with the same functionals and the somewhat larger basis set def2-SVPD.²⁵ In these calculations, all excited states up to 10 eV were determined.^{24,25} In addition, Turbomole^{26,27} was employed for the excited state calculations with the approximate coupled cluster singles and doubles (CC2)²⁸⁻³⁰ as well as the algebraic diagrammatic construction to second order methods (ADC(2)).^{31,32} Besides the unscaled methods, also the spin-component scaled (SCS) variants^{33,34} were applied. These calculations utilized also the def2-SVPD basis set²⁵ in combination with the corresponding auxiliary basis set for the resolution-of-identity (RI) approximation³⁵ and an SCF convergence criterion of 10^{-8} Hartree. Furthermore, core orbitals were frozen and only the first three excited states of singlet and triplet multiplicity were determined.

Finally wavefunction analysis was performed with the TheoDORÉ software package.^{36,37} The obtained natural transition orbitals (NTOs) were visualized with Jmol.³⁸

VIII. FURTHER RESULTS FROM EXCITED STATE CALCULATIONS

method	4CzIPN			3CzCIIPN		
	ΔE_{ST} [meV]	S_1 [eV]	T_1 [eV]	ΔE_{ST} [meV]	S_1 [eV]	T_1 [eV]
B3LYP						
TD-DFT	146	2.558	2.412	103	2.460	2.356
TDA	154	2.578	2.423	108	2.473	2.365
sTD-DFT	46	2.411	2.365	41	2.341	2.300
sTDA	56	2.421	2.365	47	2.347	2.300
CAM-B3LYP						
TD-DFT	693	3.324	2.631	589	3.259	2.670
TDA	359	3.359	3.000	232	3.279	3.047
sTD-DFT	77	3.056	2.979	49	3.013	2.964
sTDA	87	3.067	2.980	54	3.019	2.965
Post-HF						
ADC(2)	45	2.765	2.719	20	2.770	2.751
SCS-ADC(2)	42	3.115	3.072	15	3.137	3.122
CC2	43	2.842	2.798	22	2.847	2.824
SCS-CC2	38	3.179	3.140	16	3.204	3.188

TABLE II: Vertical singlet-triplet gaps and energies of the first excited singlet and triplet states relative to the optimized ground state.

To further assess the sTD-DFT and sTDA as well as the (SCS-)CC2 results, we performed additional calculations *via* regular TD-DFT with and without TDA and *via* ADC(2) with and without spin-component scaling. As summarized in table II, the computed values for the vertical energy gap between T_1 and S_1 (ΔE_{ST}) strongly depend on the choice of the functional in TD-DFT. The global hybrid functional B3LYP with 20% exact exchange overestimates

this splitting by a factor of approximately 2 relative to the experimental values, whereas the range-separated CAM-B3LYP functional yields significantly larger values. Our results for 4CzIPN corroborate the findings that the choice of functional shows a pronounced effect on ΔE_{ST} and that the results from the employed global hybrid functional are in better agreement with experiments than from the range-separated one, which have first been reported by Adachi *et al.*³⁹

Furthermore, the application of the TDA in the excited state calculations improves the results only in case of CAM-B3LYP, but the computed values for the vertical ΔE_{ST} are still much larger than with the B3LYP functional. For the latter, TDA does not lead to significant improvements. Relative to the results obtained with regular TD-DFT, the semiempirical sTD-DFT and sTDA approaches proposed by Grimme and coworkers²²⁻²⁴ yield values of ΔE_{ST} , which are in better agreement with the Post-Hartree-Fock methods. Also these values do not exhibit such a pronounced dependence on the chosen functional as for the regular TD-DFT/TDA calculations, but the individual energies of the S_1 and T_1 states behave more similar.

The origin of the good performance of the semiempirical sTD-DFT and sTDA methods for ΔE_{ST} might be traced back to the fact that they are based on regular DFT ground state calculations, but the parameters employed in the excited state calculations were fitted to reproduce excitation energies obtained from SCS-CC2 calculations.²⁴ To assess the performance and reliability of this and related Post-Hartree-Fock methods, we performed corresponding calculations for 4CzIPN and 3CzCIIPN. For this purpose, we employed the two approximate second order methods CC2 and ADC(2) with and without SCS. All four methods result in a similar value for the difference of ΔE_{ST} between 4CzIPN and 3CzCIIPN ranging from 21 to 27 meV. Furthermore, the individual values are below 50 meV. In contrast to this, the vertical excitation energies of S_1 and T_1 exhibit a larger variance of around 0.4 eV, which is reminiscent of the functional dependence in case of the DFT-based calculations. Overall, the employed second order methods result in a consistent picture for ΔE_{ST} .

IX. POPULATION ANALYSIS

To better understand the increase in charge transfer character from 4CzIPN to 3CzCIIPN, the individual populations of the excited electron and hole for the three fragments can be analyzed for each state, see table III. The hole population on fragment 1 (h_1) and the electron population on fragment 2 (e_2) increase, whereas the hole population on fragment 2 (h_2) and electron population on fragment 1 (e_1) decrease. Therefore, the hole becomes more localized on fragment 1 and the electron on fragment 2. In contrast to this, the populations on fragment 3 remain nearly constant. Therefore, also this analysis shows that the localization of the excited electron and of the hole on different fragments is favored for 3CzCIIPN relative to 4CzIPN resulting in a smaller overlap of the corresponding wavefunctions and a decrease of ΔE_{ST} .

	4CzIPN		3CzCIIPN	
	T_1	S_1	T_1	S_1
h_1	0.739	0.798	0.822	0.848
e_1	0.164	0.165	0.113	0.113
h_2	0.207	0.146	0.123	0.103
e_2	0.620	0.618	0.664	0.665
h_3	0.008	0.008	0.010	0.004
e_3	0.170	0.169	0.177	0.178

TABLE III: Electron (e) and hole (h) populations of the first excited singlet states (S_1) and the first triplet state (T_1) divided into three fragments for the two investigated molecules obtained from the SCS-CC2 calculations. The first fragment consists of the carbazole units, the second one of the benzene ring and in case of 3CzCIIPN also of the Cl atom, and the third one of the cyano groups.

-
- ¹ T. Kobayashi, A. Niwa, K. Takaki, S. Haseyama, T. Nagase, K. Goushi, C. Adachi, and H. Naito, *Physical Review Applied* **7**, 034002 (2017).
 - ² R. Dennington, T. Keith, and J. Millam, *GaussView Version 5.0.9*. Semichem Inc. Shawnee Mission KS (2009).
 - ³ A. D. Becke, *Physical Review A* **38**, 3098 (1988).
 - ⁴ C. Lee, W. Yang, and R. G. Parr, *Physical Review B* **37**, 785 (1988).
 - ⁵ A. D. Becke, *The Journal of Chemical Physics* **98**, 5648 (1993).
 - ⁶ K. Liang, C. Zheng, K. Wang, W. Liu, Z. Guo, Y. Li, and X. Zhang, *Physical Chemistry Chemical Physics* **18**, 26623 (2016).
 - ⁷ P. De Silva, *Journal of Physical Chemistry Letters* **10**, 5674 (2019).
 - ⁸ C. Wang, K. Zhou, S. Huang, and Q. Zhang, *Journal of Physical Chemistry C* **123**, 13869 (2019).
 - ⁹ W. Zhang, H. Song, J. Kong, Z. Kuang, M. Li, Q. Guo, C.-f. Chen, and A. Xia, *The Journal of Physical Chemistry C* **123**, 19322 (2019).
 - ¹⁰ S. Montanaro, A. J. Gillett, S. Feldmann, E. W. Evans, F. Plasser, R. H. Friend, and I. A. Wright, *Physical Chemistry Chemical Physics* **21**, 10580 (2019).
 - ¹¹ S. Weissenseel, N. A. Drigo, L. G. Kudriashova, M. Schmid, T. Morgenstern, K.-H. Lin, A. Prlj, C. Corminboeuf, A. Sperlich, W. Brütting, M. K. Nazeeruddin, and V. Dyakonov, *The Journal of Physical Chemistry C* **123**, 27778 (2019).
 - ¹² S. Izumi, H. F. Higginbotham, A. Nyga, P. Stachelek, N. Tohnai, P. de Silva, P. Data, Y. Takeda, and S. Minakata, *Journal of the American Chemical Society*, jacs.9b11578 (2020).
 - ¹³ S. Grimme, J. Antony, S. Ehrlich, and H. Krieg, *J. Chem. Phys.* **132**, 154104 (2010).
 - ¹⁴ S. Grimme, S. Ehrlich, and L. Goerigk, *Journal of Computational Chemistry* **32**, 1456 (2011).
 - ¹⁵ M. Moral, L. Muccioli, W. J. Son, Y. Olivier, and J. C. Sancho-Garcia, *Journal of Chemical Theory and Computation* **11**, 168 (2015).
 - ¹⁶ Y. Noguchi and O. Sugino, *Journal of Physical Chemistry C* **121**, 20687 (2017).
 - ¹⁷ W. J. Hehre, R. Ditchfield, and J. A. Pople, *J. Chem. Phys.* **56**, 2257 (1977).
 - ¹⁸ T. Yanai, D. P. Tew, and N. C. Handy, *Chemical Physics Letters* **393**, 51 (2004).
 - ¹⁹ M. J. Frisch, G. W. Trucks, H. B. Schlegel, G. E. Scuseria, M. A. Robb, J. R. Cheeseman, G. Scalmani, V. Barone, G. A. Petersson, H. Nakatsuji, X. Li, M. Caricato, A. V. Marenich, J. Bloino, B. G. Janesko, R. Gomperts, B. Mennucci, H. P. Hratchian, J. V. Ortiz, A. F. Izmaylov, J. L. Sonnenberg, D. Williams-Young, F. Ding, F. Lipparini, F. Egidi, J. Goings, B. Peng, A. Petrone, T. Henderson, D. Ranasinghe, V. G. Zakrzewski, J. Gao, N. Rega, G. Zheng, W. Liang, M. Hada, M. Ehara, K. Toyota, R. Fukuda, J. Hasegawa, M. Ishida, T. Nakajima, Y. Honda, O. Kitao, H. Nakai, T. Vreven, K. Throssell, J. A. Montgomery, Jr., J. E. Peralta, F. Ogliaro, M. J. Bearpark, J. J. Heyd, E. N. Brothers, K. N. Kudin, V. N. Staroverov, T. A. Keith, R. Kobayashi, J. Normand, K. Raghavachari, A. P. Rendell, J. C. Burant, S. S. Iyengar, J. Tomasi, M. Cossi, J. M. Millam, M. Klene, C. Adamo, R. Cammi, J. W. Ochterski, R. L. Martin, K. Morokuma, O. Farkas, J. B. Foresman, and D. J. Fox, *Gaussian 16*, Revision C.01. Gaussian Inc. Wallingford CT (2019).
 - ²⁰ F. Neese, *WIRES Comput. Mol. Sci.* **2**, 73 (2012).
 - ²¹ F. Neese, *Wiley Interdisciplinary Reviews: Computational Molecular Science* **8**, e1327 (2018).
 - ²² S. Grimme, *The Journal of Chemical Physics* **138**, 244104 (2013).
 - ²³ C. Bannwarth and S. Grimme, *Computational and Theoretical Chemistry* **1040-1041**, 45 (2014).
 - ²⁴ T. Risthaus, A. Hansen, and S. Grimme, *Phys. Chem. Chem. Phys.* **16**, 14408 (2014).
 - ²⁵ D. Rappoport and F. Furche, *Journal of Chemical Physics* **133**, 134105 (2010).
 - ²⁶ F. Furche, R. Ahlrichs, C. Hättig, W. Klopper, M. Sierka, and F. Weigend, *Wiley Interdisciplinary Reviews: Computational Molecular Science* **4**, 91 (2014).
 - ²⁷ TURBOMOLE V7.2 2017, a development of University of Karlsruhe and Forschungszentrum Karlsruhe GmbH, 1989-2007, TURBOMOLE GmbH, since 2007. Available from <http://www.turbomole.com> (Accessed: 23/01/2020).
 - ²⁸ O. Christiansen, H. Koch, P. Jørgensen, and T. Helgaker, *Chemical Physics Letters* **263**, 530 (1996).
 - ²⁹ C. Hättig and F. Weigend, *Journal of Chemical Physics* **113**, 5154 (2000).
 - ³⁰ C. Hättig and K. Hald, *Physical Chemistry Chemical Physics* **4**, 2111 (2002).
 - ³¹ A. B. Trofimov and J. Schirmer, *Journal of Physics B: Atomic, Molecular and Optical Physics* **28**, 2299 (1995).
 - ³² C. Hättig, *Advances in Quantum Chemistry* **50**, 37 (2005).
 - ³³ S. Grimme, *Journal of Chemical Physics* **118**, 9095 (2003).
 - ³⁴ A. Hellweg, S. A. Grün, and C. Hättig, *Physical Chemistry Chemical Physics* **10**, 4119 (2008).
 - ³⁵ A. Hellweg and D. Rappoport, *Physical Chemistry Chemical Physics* **17**, 1010 (2015).
 - ³⁶ F. Plasser and H. Lischka, *Journal of Chemical Theory and Computation* **8**, 2777 (2012).
 - ³⁷ F. Plasser, *TheoDORE 1.6: a package for theoretical density, orbital relaxation, and exciton analysis*. Available from <http://theodore-qc.sourceforge.net> (Accessed: 23/01/2020).
 - ³⁸ Jmol: an open-source Java viewer for chemical structures in 3D, <http://www.jmol.org/> (Accessed: 23/01/2020).
 - ³⁹ H. Uoyama, K. Goushi, K. Shizu, H. Nomura, and C. Adachi, *Nature* **492**, 234 (2012).